J. Opt. A: Pure Appl. Opt. **10** (2008) 104019 (9pp) doi:10.1088/1464-4258/10/10/104019

# Monitoring of atmospheric trace gases, clouds, aerosols and surface properties from UV/vis/NIR satellite instruments

**T Wagner[1], S Beirle[1], T Deutschmann[2], E Eigemeier[1], C Frankenberg[3], M Grzegorski[2], C Liu[1], T Marbach[1], U Platt[2] and M Penning de Vries[1]**

[1] Max Planck Institute for Chemistry, Joh.-Joachim-Becher-Weg 27, D-55128, Mainz, Germany
[2] Institut für Umweltphysik, University of Heidelberg, INF 229, D-69120, Germany
[3] SRON, Sorbonnelaan 2, 3584 CA Utrecht, The Netherlands

Received 7 March 2008, accepted for publication 23 May 2008
Published 28 August 2008
Online at stacks.iop.org/JOptA/10/104019

**Abstract**
A new generation of UV/vis/near-IR satellite instruments like GOME (since 1995), SCIAMACHY (since 2002), OMI (since 2004), and GOME-2 (since 2006) have allowed one to measure backscattered solar radiance from the Earth with moderate spectral resolution over a large wavelength range (240–790 nm). The SCIAMACHY instrument also includes additional spectral channels in the near-IR. From the measured spectra several important stratospheric and tropospheric trace gases (e.g. $O_3$, $NO_2$, OClO, HCHO, $SO_2$, BrO, $H_2O$) as well as clouds, aerosols and surface properties can be determined from space. Because of its extended spectral range, the SCIAMACHY instrument also allows the retrieval of greenhouse gases ($CO_2$, $CH_4$) and CO in the near-IR. Almost all of the tropospheric trace gases have been observed by these instruments for the first time. From satellite data it is possible to investigate their temporal and spatial variation. Also, different sources can be characterized and quantified. The derived global distributions can serve as input and for the validation of atmospheric models. Here we give an overview of the current status of these new instruments and data products and their recent applications in the investigation of various atmospheric and oceanic phenomena.

**Keywords:** satellite remote sensing, atmospheric composition

(Some figures in this article are in colour only in the electronic version)

## 1. Introduction

In order to make reliable predictions of future changes of climate and air quality, numerical computer simulations are usually performed. These simulations are based on our current understanding of the physics and chemistry as well as on the dynamics of the atmosphere and oceans. Also the interactions between the different parts of the Earth system, like atmosphere, ocean, cryosphere, etc, are considered. Typically the outputs of these models are four-dimensional fields of constituent concentrations (e.g. air pollutants, greenhouse gases, aerosols, clouds) together with radiative properties. To check the validity of the model simulations, it is important to compare these fields to measurements. For the atmosphere, a large variety of *in situ* and remote sensing techniques can be used for the comparison, with each technique having specific advantages and disadvantages. Compared to other kinds of measurements, satellite observations have the advantage that they provide global observations and allow us to retrieve information from remote regions (often for the first time). In addition, they typically yield integrated quantities, e.g. the vertically integrated trace gas concentration. Together with the global coverage, this capability ensures that satellite observations typically do not miss important information (e.g. from a specific location). Information on spatial patterns can also be derived from satellite observations. In this way it is often possible to directly assign a specific origin to an observed phenomenon (e.g. enhanced trace gas concentrations

 

**Table 1.** Properties of the different satellite instruments.

| Instrument/satellite | Launch | Wavelength range | Viewing geometries | Time for global coverage (nadir) (days) | Spatial resolution (nadir) (km$^2$) |
|---|---|---|---|---|---|
| GOME/ERS-2 | 1995 | 240–790 nm | Nadir (±30°) | 3 | 40 × 320 |
| SCIAMACHY/ENVISAT | 2002 | 240–2380 nm (with gaps) | Nadir (±30°), limb, occultation | 6 | 30 × 60 |
| OMI/AURA | 2004 | 270–500 nm | Nadir (±60°) | 1 | 13 × 24 |
| GOME-2/METOP | 2006 | 240–790 nm | Nadir (±30°) | 1.5 | 40 × 80 |

above an industrialized area). Also, direct comparisons between observations at different locations become possible. In addition, satellite instruments are typically very stable and allow trends to be determined on a global scale (e.g. the increase of pollutants or greenhouse gases). Major limitations of satellite observations are their relatively large measurement uncertainty, their coarse spatial resolution and rare sampling.

Here we give an overview of the analysis of trace gas distributions as well as aerosol and cloud properties from modern UV/vis/near-IR satellite instruments. Like the TOMS instruments, these satellite instruments were primarily designed for the observation of the stratospheric ozone layer. However, in this paper we focus on the analysis of tropospheric species; detailed information about retrievals on stratospheric ozone (total columns and profiles) can be found in [1–4], for example, and references therein.

In addition to the atmospheric products, information on surface properties (e.g. vegetation type) can also be derived. We discuss the major processing steps, show images with the average global distributions and present selected case studies. Finally we give an outlook on future developments.

## 2. Instruments

The global ozone monitoring experiment (GOME) is one of several instruments aboard the European research satellite ERS-2 [1], which was launched in 1995. It consists of a set of four spectrometers that simultaneously measure sunlight reflected from the Earth's atmosphere and from the ground in four spectral windows covering the wavelength range between 240 and 790 nm with moderate spectral resolution (0.2–0.4 nm full width at half maximum (FWHM)). The satellite operates in a nearly polar, sun-synchronous orbit at an altitude of 780 km with a local equator crossing time at approximately 10:30. While the satellite orbits in an almost north–south direction, the GOME instrument scans the surface in the perpendicular, east–west direction. During one sweep, three individual spectral scans are performed. The corresponding three ground pixels (a western, a central, and an eastern pixel) lie side by side, each covering an area of 320 km (east–west) by 40 km (north–south). The Earth's surface is totally covered within 3 days. In 2002 the SCanning Imaging Absorption SpectroMeter for Atmospheric CartograpHY (SCIAMACHY) [5] was launched on board ENVISAT. In addition to GOME it measures in a wider wavelength range (240–2380 nm) including the absorption features of several greenhouse gases ($CO_2$, $CH_4$, $N_2O$) and CO in the near-IR. It operates in different viewing modes (nadir, limb, occultation), which also allow stratospheric trace gas profiles to be derived. Another advantage is that the ground pixel size for the nadir viewing mode was significantly reduced to 30 × 60 km$^2$ (in a special mode even to 15 × 30 km$^2$). This is very important for the observation of tropospheric trace gases because of the strong spatial gradients occurring for such species. In addition, the ozone monitoring instrument (OMI) was launched on AURA in 2004. Like GOME it operates only in nadir geometry. It has a reduced spectral range (270–500 nm), but a finer spatial resolution (up to 13 × 16 km$^2$) and daily global coverage [6]. Recently, the first GOME-2 instrument (in total three instruments are scheduled) was launched on METOP in 2006. It is similar to the GOME-1 instrument, but with finer spatial resolution (40 × 80 km$^2$) and almost daily global coverage [7]. An overview on the instrumental properties is given in table 1.

## 3. Trace gas data analysis

From the raw satellite spectra the absorptions of the individual atmospheric trace gases are determined using differential optical absorption spectroscopy (DOAS) [8]. In brief, the measured spectra are modeled with a nonlinear fitting routine that suitably weights the known absorption spectra of atmospheric trace gases and a solar background spectrum, frequently called the solar Fraunhofer reference spectrum. Also, the influence of atmospheric Raman scattering (the so-called Ring effect) is considered [9, 10]. Contributions of atmospheric broadband extinction processes (e.g. Rayleigh and Mie scattering) are removed from the spectrum by fitting a polynomial of low order. More details on the spectral analysis can be found in [11]. In figure 1 the wavelength ranges are indicated where the different atmospheric trace gases (and also cloud and surface properties) are analyzed. For each species, spectral regions are selected where the most prominent differential absorption structures appear or/and the smallest spectral interferences with other species are expected. In figure 1 the results of the spectral analysis are also presented. The yellow lines indicate the absorption spectra of the respective trace gas scaled to the absorptions determined in the GOME spectrum (blue lines). From the inferred absorption, and knowledge of the differential (narrow-band) absorption cross sections, the trace gas slant column density (SCD, the integrated trace gas concentration along the absorption path) is calculated. It should be noted that for cases of strong absorbers (optical depth > about 0.1), the normal

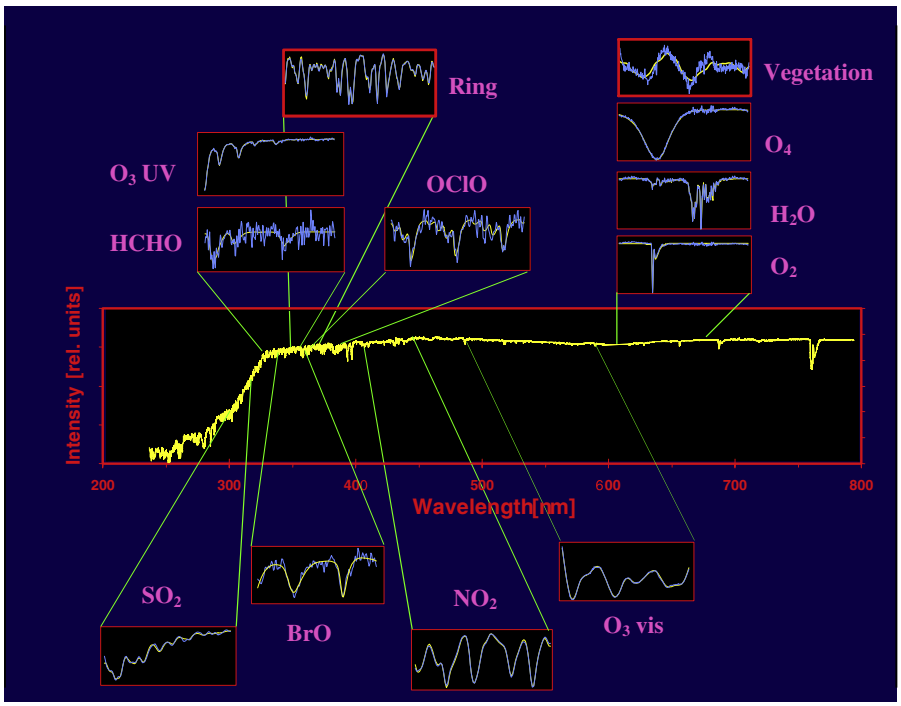


**Figure 1.** Selection of wavelength ranges for the spectral analysis of the different trace gases analyzed from GOME spectra. The yellow lines indicate the absorption spectra of the trace gases scaled to the absorptions determined in the satellite spectrum (light blue lines). In the same way as the trace gas absorption, the spectral reflection features of various vegetation types and the Ring effect can also be analyzed. In the near-IR (not shown) the absorptions of $CH_4$, $CO_2$, and CO can be analyzed.

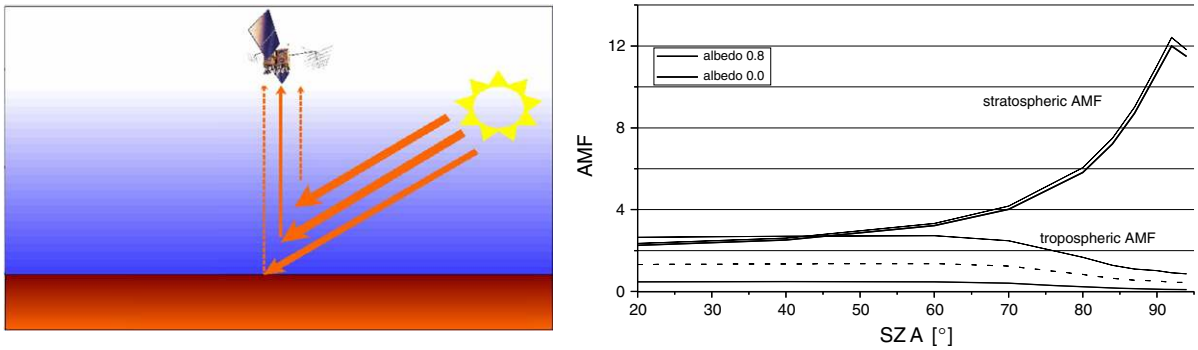


**Figure 2.** Left: viewing geometry for satellite observations in nadir mode. The received sunlight is scattered by the atmosphere and reflected from the ground. Right: influence of the ground albedo on the AMFs for trace gas profiles in the stratosphere (maximum concentration at 14 km) and the lower troposphere (constant concentration in the boundary layer between the surface and 1 km). In contrast to the stratospheric AMF, the tropospheric AMF depends strongly on the ground albedo. The dashed line shows the AMF which is appropriate for trace gases in the boundary layer. It is calculated assuming a ground albedo of 0.8 and a geometric cloud fraction of 0.5.

DOAS approach is no longer valid. Thus for the analysis of $O_3$, $H_2O$, $CO_2$, and $CH_4$, modified DOAS algorithms have been developed (e.g. [3, 12–14]).

For the interpretation of the obtained SCD, radiative transfer modeling (RTM) is performed. Typically the results of RTM are expressed as air mass factors (AMF), where AMF = SCD/VCD (with VCD the vertical column density, the vertically integrated trace gas concentration). In a rough, first approximation the AMF is given by the ratio of the path length of the sunlight through the atmosphere and the vertical path, i.e. AMF $\approx 1/\cos(\mathrm{SZA}) + 1/\cos(\mathrm{EAO})$ with SZA the solar zenith angle and EAO the elevation angle of the observation. We calculate AMFs using the Monte Carlo RTM TRACY-2, which includes spherical geometry and multiple scattering [15, 16]. The AMF mainly depends on the SZA, the atmospheric concentration profile of the measured species and the ground albedo.

In figure 2, examples of AMFs for stratospheric and tropospheric profiles are displayed. The AMF for the trace gases located in the stratosphere ($\mathrm{AMF_{strat}}$) strongly increases toward high SZA; in contrast, the AMF for species in the lower troposphere ($\mathrm{AMF_{trop}}$) shows only a weak SZA dependence. While for SZA $\leqslant 87°$ the $\mathrm{AMF_{strat}}$ can be calculated with high accuracy, the calculations for $\mathrm{AMF_{trop}}$ show large uncertainties

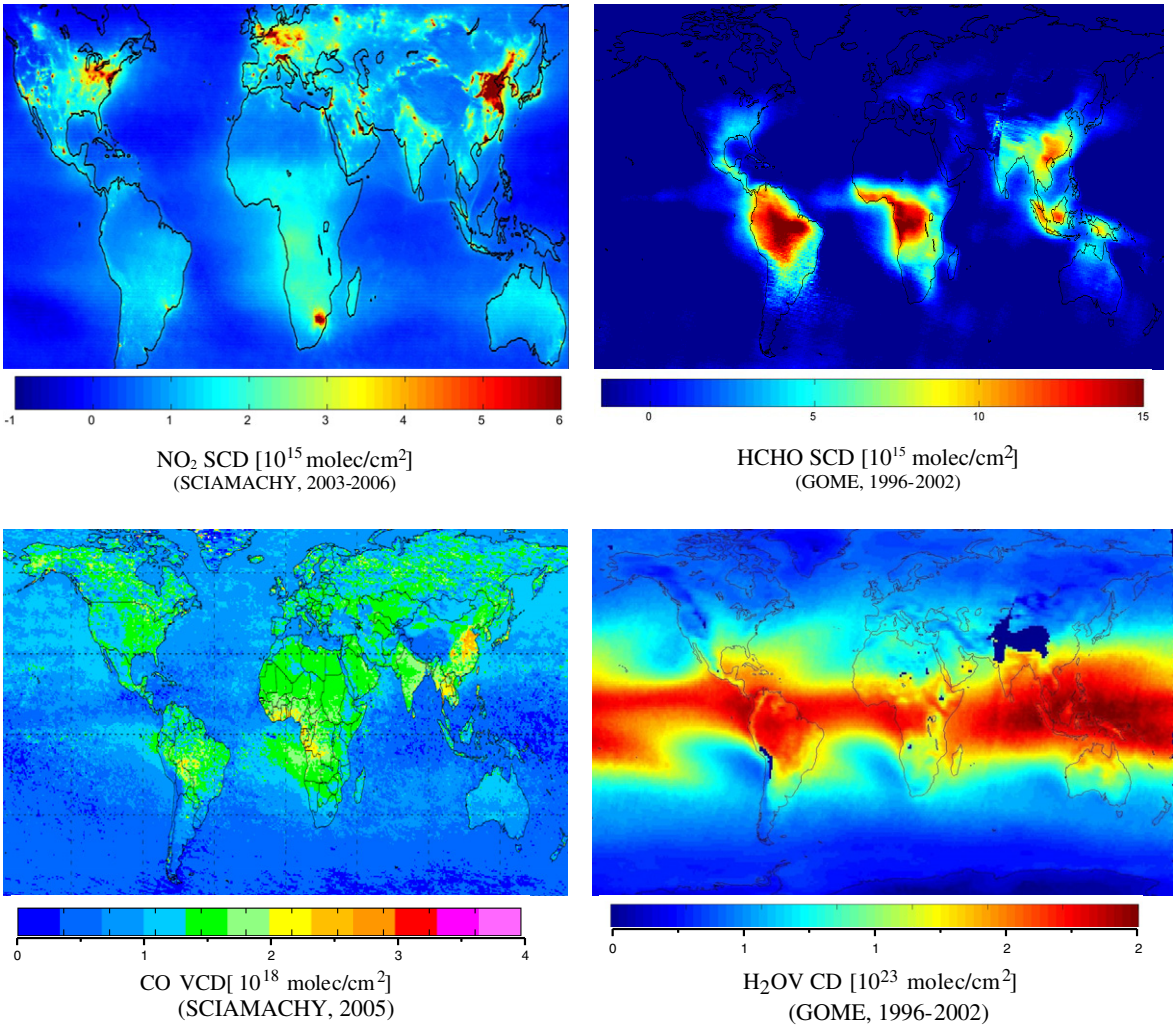


**Figure 3.** Global distributions of tropospheric $NO_2$, HCHO, CO and $H_2O$. The observed patterns indicate the locations of major sources. The distribution of water vapor is mainly determined by the atmospheric temperature.

for several reasons:

(1) Because of the high air pressure and high (and variable) aerosol concentration in the troposphere, the influence of multiple scattering is large compared to the stratosphere.
(2) The influence of the ground albedo on the sensitivity (and accordingly the respective AMF) of the satellite observations to tropospheric species is strong compared to the stratosphere (see figure 2). $AMF_{trop}$ is small when the ground albedo is low (e.g. above the ocean) and large when the ground albedo is high (e.g. over snow and ice).
(3) Clouds can shield absorbing species which are located below the cloud cover. This effect is in particular strong when the ground albedo is low (e.g. above the ocean).

Because of these uncertainties, the quantitative determination of tropospheric trace gases from satellite observations with high accuracy is only possible when precise information about the above mentioned parameters is available. This is in general not the case for a single observation. However, when satellite observations are spatially and temporally averaged the uncertainties can decrease significantly. Information on clouds can also be determined from the satellite observations. Besides the measured radiance, the absorptions of the oxygen molecule $O_2$ and dimer $O_4$ also hold information on cloud fraction and cloud top height [17–19]. In addition, the amount of Raman scattering (the so-called Ring effect) can also be investigated; this depends strongly on the cloud fraction and cloud altitude [20] (see also section below). More information on AMF for tropospheric species can be found in [21–23].

Several tropospheric trace gases like $NO_2$, HCHO, BrO, $SO_2$, $H_2O$, glyoxal, CO, $CH_4$, $CO_2$ and IO are currently retrieved from satellite observations. Here we show some examples which illustrate the potential of these new data sets. In figure 3 the global distributions of tropospheric $NO_2$, formaldehyde (HCHO), carbon monoxide (CO) and water vapor ($H_2O$) are shown. $NO_2$ is a pollutant which affects human health and controls ozone chemistry. HCHO is an indicator for photochemical activity in the atmosphere. It is produced during the degradation of methane (and many other hydrocarbons). Large amounts of HCHO are also observed over regions of strong biomass burning. CO is produced by biomass burning, traffic and industrial processes. Water

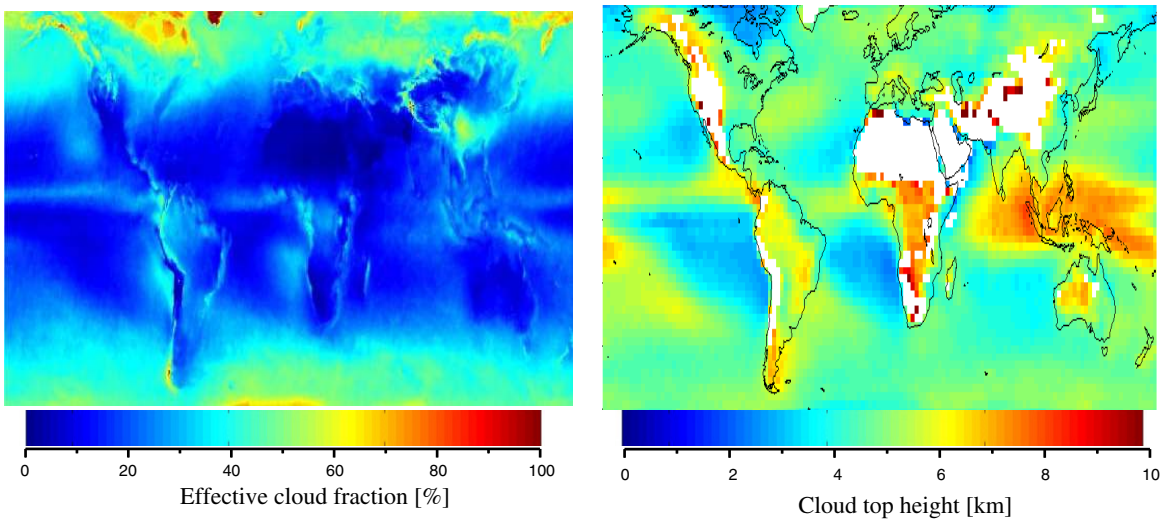


**Figure 4.** Average cloud properties (1996–2002) retrieved from GOME observations. Left: effective cloud fraction derived from radiance measurements in the green and red spectral range. Right: effective cloud top height derived from observations of $O_2$ absorption and the effective cloud fraction. Over some regions (white areas) with low effective cloud fraction and high surface elevation no meaningful inversion of the cloud top height is possible with our current version of the algorithm.

vapor distribution is controlled by evaporation, transport and precipitation processes. Water vapor is important for many aspects of atmospheric physics and chemistry; in particular it is the most important natural greenhouse gas.

## 4. Cloud and aerosol data analysis

The most obvious effect of clouds on satellite observations is that they increase the backscattered radiance because of additional scattering by the cloud particles. Thus the fractional cloud cover can be determined from the observed radiance [24–26]. From GOME and SCIAMACHY we retrieve in this way a so-called effective cloud fraction using the HICRU algorithm [26]. The HICRU effective cloud fraction depends on both the geometrical cloud fraction and the cloud top albedo (mainly depending on cloud optical thickness). The HICRU cloud fraction (see figure 4) is representative of the geometrical cloud fraction of a cloud with cloud top albedo of ∼80%.

Besides the cloud fraction, information on the cloud top height can also be retrieved. Since the atmospheric concentration of oxygen changes only slightly with air pressure and temperature, variations in the measured absorptions of the oxygen molecule $O_2$ or dimer $O_4$ are a direct indication of modifications of radiative transport through the atmosphere (e.g. due to clouds or aerosols). Examples of the spectral retrieval of the $O_2$ and $O_4$ absorptions are also shown in figure 1. In the presence of clouds, these absorptions are typically reduced because of the shielding effect of clouds for the atmospheric layers below. Figure 4 shows the average global distribution of cloud top height, derived from the $O_2$ absorption and the effective cloud fraction [19]. Note that like for the trace gas analyses, for the retrieval of the cloud top height radiative transfer modeling also has to be applied. From a comparison of these cloud top heights to those analyzed from thermal IR satellite observations, e.g. for the International Satellite Cloud Climatology Project (ISCCP [24, 25]), a good qualitative agreement for the global patterns was found, but the absolute values often show systematic differences [19]. Such systematic differences should, however, be expected because both methods are based on completely different physical principles. Similar algorithms were developed in [17, 18].

Additional information on cloud top height can be also found from the analysis of the Ring effect [20]. Atmospheric Raman scattering leads to a filling-in of solar Fraunhofer lines in the measured spectra, which can be quantitatively analyzed by including a so-called Ring spectrum [9, 10] in the DOAS analysis (see figure 1). Using radiative transfer modeling, the observed strength of the Ring effect can be inverted into an effective cloud top height [20].

In the UV, visible and near-IR spectral range, the probability of light scattering by cloud particles has little or no dependence on wavelength. Also, the absorption by cloud particles is negligibly weak. In both aspects, aerosol particles can have systematically different properties. Usually, the probability for a photon to be scattered by aerosols increases with decreasing wavelength. In addition, aerosol particles (especially biomass burning aerosols or desert dust aerosols) can strongly absorb the sunlight in the atmosphere. Because of both effects, aerosols are typically 'colored' (e.g. the bluish smoke of a fire) and can thus be detected by their specific wavelength dependences in the measured spectra of backscattered sunlight. One well established aerosol product analyzed from the UV spectral range is the so-called aerosol absorbing index, which can also be analyzed in the presence of clouds (e.g. [27, 28]). High values are observed for regions with enhanced concentrations of desert dust or biomass-burning aerosols (see figure 5). Also algorithms for other aerosol properties (e.g. optical depth of extinction and absorption) have been developed (e.g. [29] and references therein). Like for clouds, information on the altitude

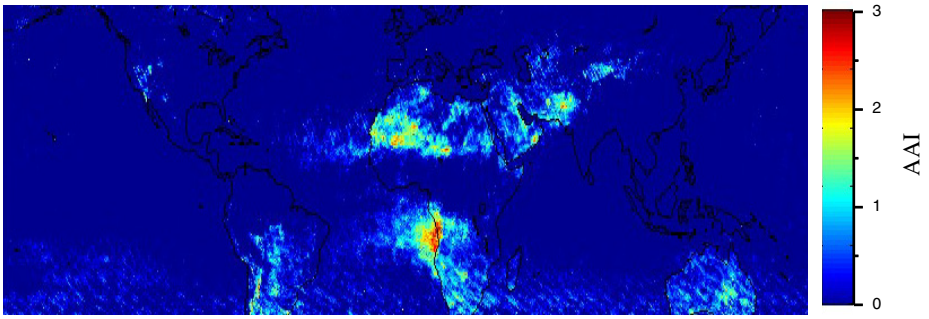


**Figure 5.** Aerosol absorbing index for July–September 2004 derived from SCIAMACHY observations. Enhanced values are found for regions with desert dust or biomass-burning aerosols.

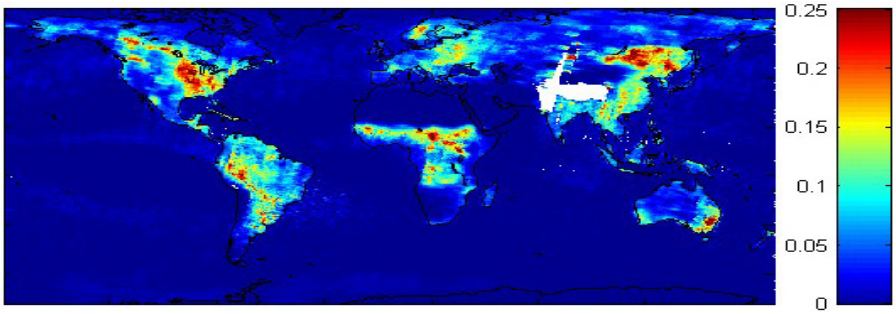


**Figure 6.** GOME vegetation index for grass averaged for September 1998.

distribution of the aerosol load can also in principle be derived from the measured absorptions of $O_2$ and $O_4$.

## 5. Vegetation type data analysis

Algorithms for the remote sensing of vegetation have been developed and successfully applied to satellite observations for a long time. Typically they are based on the measured radiance in the red and near-IR part of the spectrum. Over this wavelength range, the reflectivity of vegetation changes strongly, caused by the absorption of various kinds of chlorophyll and pigments. Thus a clear vegetation signal can easily be derived. Definitions of vegetation indices based on intensity ratios can be found in [30], for example.

Recently, a new vegetation algorithm was developed in our group, which can be applied to new satellite sensors with moderate spectral resolution [31]. In contrast to the existing algorithms, this method exploits the narrow-band spectral information of the vegetation reflectance, which in particular allows different types of vegetation to be discriminated. One additional advantage is that the influence of atmospheric absorption is automatically corrected. The retrieval of the vegetation signal is performed in a similar way as the trace gas analyses. The spectra of vegetation reflectance are included in the DOAS analysis of the measured spectra [31] (see figure 1). In figure 6 an example of the global distribution of the grass spectral reflection signal analyzed in GOME spectra is shown. It should be noted that the spectral albedo of the Earth's surface [32] and ocean properties [31, 33, 34] have also been analyzed from the satellite spectra.

## 6. Selected applications

The information on the global distribution of atmospheric trace gases (and other properties) can be utilized in various ways. One important possibility is to compare the satellite results with spatial patterns derived from other sources; one example is shown in figure 7. The tropospheric $NO_2$ distribution is compared to the distribution of ship traffic. To make the spatial structures in the $NO_2$ observations clearer, high-pass filtering in latitudinal and longitudinal directions was applied. The $NO_x$ emissions caused by ship traffic are clearly visible in the satellite observations. Although the enhancements are small, they can be unambiguously assigned to the emissions of ships. In this way, it was possible to derive a completely independent estimate of the $NO_x$ emissions from ships [35].

Another possibility is to investigate the weekly cycle of trace gas amounts at specific locations [36]. From the amplitude of the decrease at weekends information about the anthropogenic influence on these pollutants can be estimated. In figure 8 the weekly cycle of the $NO_2$ VCD over São Paulo as derived from GOME observations is presented. Also shown is the spatial distribution of tropospheric $NO_2$ over South America analyzed from the SCIAMACHY instrument (note the different color scale compared to figure 3).

Another selected example takes advantage of the fact that UV/vis satellite observations of water vapor have similar sensitivity over land and ocean. Thus continuous global patterns and their temporal variation can be investigated. In figure 9 the relative anomaly of the global water vapor

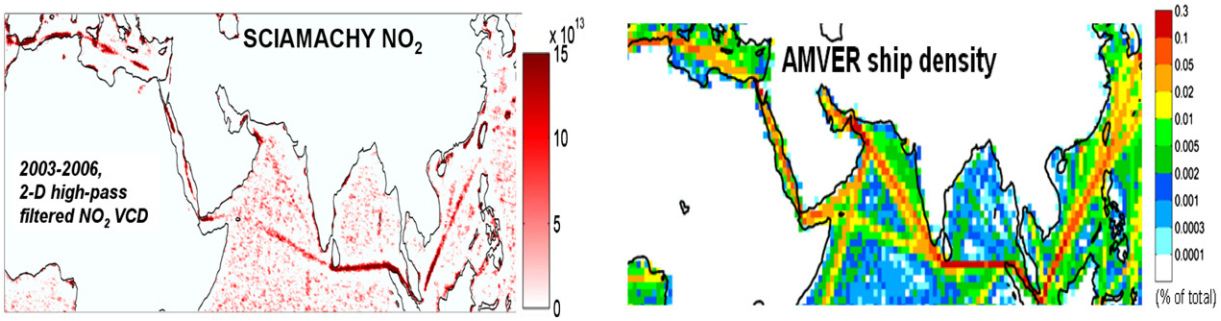


**Figure 7.** Tropospheric $NO_2$ distribution derived from satellite observations (left) and ship traffic density (right).

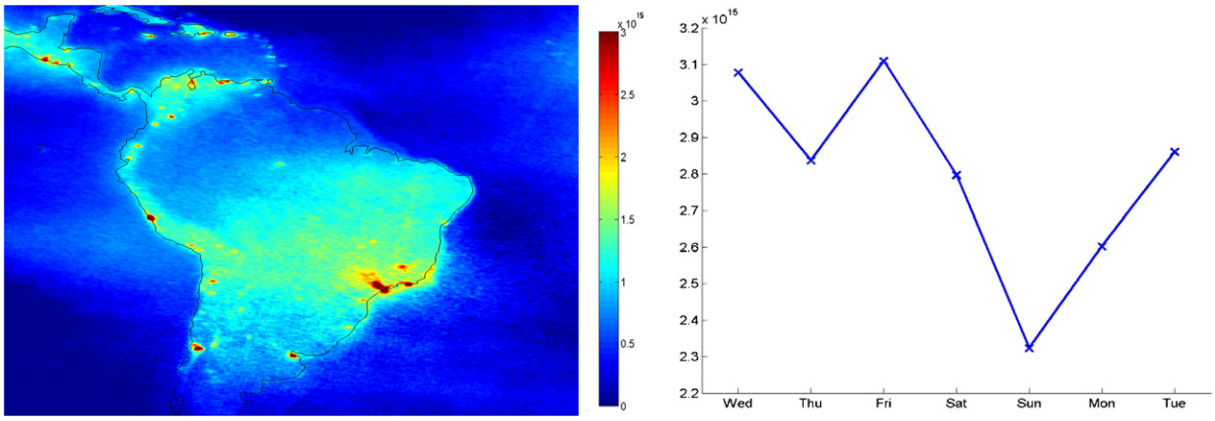


**Figure 8.** Left: distribution of tropospheric $NO_2$ VCD over South America as derived from SCIAMACHY measurements. Right: weekly cycle of tropospheric $NO_2$ over São Paulo, analyzed from 4 years of SCIAMACHY observations.

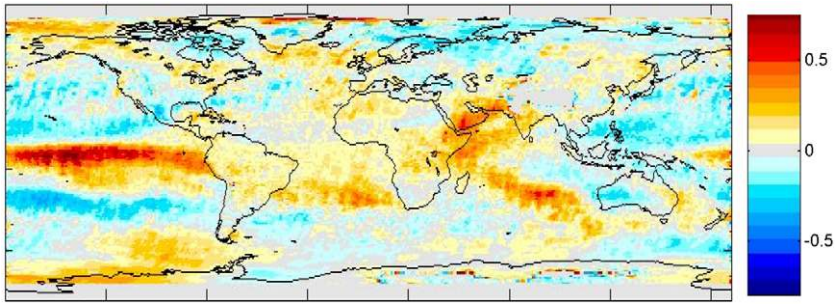


**Figure 9.** Relative anomalies (average from October 1997 to March 1998) of the total column precipitable water during the El-Niño period with respect to the average of the non-El-Niño years (1996/97, 1998/99, 1999/2000, 2000/01). Significant El-Niño induced anomalies are found not only for the tropics but also for mid and high latitudes. The maps cover the latitude and longitude ranges 90° S–90° N and 180° W–180° E.

distribution during the strong El-Niño–Southern Oscillation (ENSO) event in 1997/98 with respect to normal years is shown. Besides strong positive anomalies over the warm central Pacific, significant anomalies (positive or negative) are also found over many other parts of the globe [37]. It should be noted that tropospheric water vapor products are also derived from satellite observations in the thermal IR and microwave spectral range [38]. The microwave results in particular have very high accuracy and are not affected by clouds (but are restricted to the oceans). We compared the $H_2O$ data set from GOME to microwave observations over the oceans and found very good agreement [37].

## 7. Conclusions and outlook

We have demonstrated that a variety of atmospheric trace gases and properties of clouds, aerosol and the surface can be retrieved from the spectra measured by UV/vis/near-IR satellite instruments. From these new instruments, it is possible to monitor and investigate several important atmospheric phenomena on a global scale (e.g. anthropogenic and natural emissions of pollutants and greenhouse gases). Because of the long operational time of GOME and its successors (since 1995), it is in particular possible to derive trends over a period of now more than 12 years. The planned series of GOME-2

satellite instruments will hopefully extend this range until about the year 2020. Future improvements in tropospheric data analyses will mainly address the improvement of correction of the effects of clouds. For that purpose in particular the combined analysis of atmospheric $O_2$ and $O_4$ absorptions and the Ring effect can be used.

## Acknowledgments

We would like to thank the European Space Agency (ESA) operation center in Frascati (Italy) and the 'Deutsches Zentrum für Luft- und Raumfahrt' (DLR, Germany) as well as EUMETSAT in Darmstadt for making the satellite spectral data available.

## References

[1] Burrows J P *et al* 1999 The global ozone monitoring experiment (GOME): mission concept and first scientific results *J. Atmos. Sci.* **56** 151–75

[2] Weber M, Dhomse S, Wittrock F, Richter A, Sinnhuber B-M and Burrows J P 2003 Dynamical control of NH and SH winter/spring total ozone from GOME observations in 1995–2002 *Geophys. Res. Lett.* **30** 11

[3] Van Roozendael M *et al* 2006 Ten years of GOME/ERS-2 total ozone data—the new GOME data processor (GDP) version 4: 1. Algorithm description *J. Geophys. Res.* **111** D14311

[4] Meijer Y J *et al* 2006 Evaluation of global ozone monitoring experiment (GOME) ozone profiles from nine different algorithms *J. Geophys. Res.* **111** D21306

[5] Bovensmann H, Burrows J P, Buchwitz M, Frerick J, Noël S, Rozanov V V, Chance K V and Goede A H P 1999 SCIAMACHY—mission objectives and measurement modes *J. Atmos. Sci.* **56** 127–50

[6] Levelt P F and Noordhoek R 2002 OMI algorithm theoretical basis document volume I: OMI instrument, level 0-1b processor, calibration and operations *Tech. Rep. ATBD-OMI-01* Version 1.1, August

[7] EUMETSAT 2005 *GOME-2 Products Guide* http://www.eumetsat.int/en/area4/eps/product_guides/GOME-2/GOME2-PG.pdf

[8] Platt U 1994 Differential optical absorption spectroscopy (DOAS) *Air Monitoring by Spectroscopic Techniques* (*Chemical Analysis Series* vol 127) ed M W Sigrist (New York: Wiley)

[9] Solomon S, Schmeltekopf A L and Sanders R W 1987 On the interpretation of zenith sky absorption measurements *J. Geophys. Res.* **92** 8311–9

[10] Vountas M, Rozanov V V and Burrows J P 1998 Ring-effect: impact of rotational Raman scattering on radiative transfer in earth's atmosphere *J. Quant. Spectrosc. Radiat. Transfer.* **60** 943–61

[11] Wagner T, Beirle S, Grzegorski M and Platt U 2006 Global trends (1996–2003) of total column precipitable water observed by global ozone monitoring experiment (GOME) on ERS-2 and their relation to near-surface temperature *J. Geophys. Res.* **111** D12102

[12] Buchwitz M, Rozanov V V and Burrows J P 2000 A near infrared optimized DOAS method for the fast global retrieval of atmospheric $CH_4$, CO, $CO_2$, $H_2O$ and $N_2O$ total column amounts from SCIAMACHY/ENVISAT-1 nadir radiances *J. Geophys. Res.* **105** 15231–45

[13] Frankenberg C, Platt U and Wagner T 2005 Iterative maximum a posteriori (IMAP)-DOAS for retrieval of strongly absorbing trace gases: model studies for $CH_4$ and $CO_2$ retrieval from near infrared spectra of SCIAMACHY onboard ENVISAT *Atmos. Chem. Phys.* **5** 9–22

[14] Frankenberg C, Platt U and Wagner T 2005 Retrieval of CO from SCIAMACHY onboard ENVISAT: detection of strongly polluted areas and seasonal patterns in global CO abundances *Atmos. Chem. Phys.* **5** 1639–44

[15] Deutschmann T and Wagner T 2008 *TRACY-II Users manual* http://joseba.mpch-mainz.mpg.de/tdeutschmann/tracy_II/

[16] Wagner T *et al* 2007 Comparison of box-air-mass-factors and radiances for multiple-axis differential optical absorption spectroscopy (MAX-DOAS) geometries calculated from different UV/visible radiative transfer models *Atmos. Chem. Phys.* **7** 1809–33

[17] Kuce A and Chance K V 1994 Analysis of cloud top height and cloud coverage from satellites using the $O_2$ A and B bands *J. Geophys. Res.* **99** 14481–91

[18] Koelemeijer R B A, Stammes P, Hovenier J W and de Haan J F 2001 A fast method for retrieval of cloud parameters using oxygen A band measurements from the global ozone monitoring experiment *J. Geophys. Res.* **106** 3475–90

[19] Wagner T, Beirle S, Deutschmann T, Grzegorski M and Platt U 2008 Dependence of cloud fraction and cloud top height on surface temperature derived from spectrally resolved UV/vis satellite observations *Atmos. Chem. Phys.* **8** 2299–312

[20] Joiner J and Bhartia P K 1995 The determination of cloud pressures from rotational Raman scattering in satellite backscatter ultraviolet measurements *J. Geophys. Res.* **100** 23019–26

[21] Richter A and Burrows J P 2002 Tropospheric $NO_2$ from GOME measurements *Adv. Space Res.* **29** 1673–83

[22] Eskes H J and Boersma K F 2003 Averaging kernels for DOAS total-column satellite retrievals *Atmos. Chem. Phys.* **3** 1285–91

[23] Martin R V *et al* 2002 An improved retrieval of tropospheric nitrogen dioxide from GOME *J. Geophys. Res.* **107** 4437

[24] Schiffer R A and Rossow W B 1983 ISCCP: the first project of the world climate research program *Bull. Am. Meteorol. Soc.* **64** 770–84

[25] Rossow W B and Schiffer R A 1999 Advances in understanding clouds from ISCCP *Bull. Am. Meteorol. Soc.* **80** 2261–87

[26] Grzegorski M *et al* 2006 The Heidelberg iterative cloud retrieval utilities (HICRU) and its application to GOME data *Atmos. Chem. Phys.* **6** 4461–76

[27] Herman J R, Bhartia P K, Torres O, Hsu C and Celarier E A 1997 Global distribution of UV-absorbing aerosols from Nimbus 7/TOMS data *J. Geophys. Res.* **102** D14

[28] de Graaf M and Stammes P 2005 SCIAMACHY absorbing aerosol index—calibration issues and global results from 2002–2004 *Atmos. Chem. Phys. Discuss.* **5** 3367–89

[29] Torres O, Tanskanen A, Veihelmann B, Ahn C, Braak R, Bhartia P K, Veefkind P and Levelt P 2007 Aerosols and surface UV products from ozone monitoring instrument observations: an overview *J. Geophys. Res.* **112** D24S47

[30] Birth G S and McVey G 1968 Measuring the color growing turf with a reflectance spectrophotometer *Agronomy J.* **60** 640–3

[31] Wagner T, Beirle S, Grzegorski M and Platt U 2007 Satellite monitoring of different vegetation types by differential optical absorption spectroscopy (DOAS) in the red spectral range *Atmos. Chem. Phys.* **7** 69–79

[32] Koelemeijer R B A, de Haan J F and Stammes P 2003 A database of spectral surface reflectivity in the range 335–772 nm derived from 5.5 years of GOME observations *J. Geophys. Res.* **108** 4070

[33] Vasilkov A P, Joiner J, Gleason J and Bhartia P K 2002 Ocean Raman scattering in satellite backscatter UV measurements *Geophys. Res. Lett.* **29** 1837

[34] Vountas M, Richter A, Wittrock F and Burrows J P 2003 Inelastic scattering in ocean water and its impact on trace gas retrievals from satellite data *Atmos. Chem. Phys.* **3** 1365–75

[35] Beirle S, Platt U, von Glasow R, Wenig M and Wagner T 2004 Estimate of nitrogen oxide emissions from shipping by satellite remote sensing *Geophys. Res. Lett.* **31** L18102

[36] Beirle S, Platt U, Wenig M and Wagner T 2003 Weekly cycle of NO2 by GOME measurements: a signature of anthropogenic sources *Atmos. Chem. Phys.* **3** 2225–32

[37] Wagner T, Beirle S, Grzegorski M, Sanghavi S and Platt U 2005 El-Niño induced anomalies in global data sets of water vapour and cloud cover derived from GOME on ERS-2 *J. Geophys. Res.* **110** D15104

[38] Stephens G L, Jackson D L and Bates J J 1994 A comparison of SSM/I and TOVS column water vapor data over the global oceans *Meteorol. Atmos. Phys.* **54** 183–201